Talanta 240 (2022) 123118

Contents lists available at ScienceDirect

Talanta

journal homepage: www.elsevier.com/locate/talanta

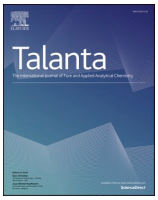

Colorimetry /SERS dual-sensor of H_2O_2 constructed via TMB–Fe_3O_4@ AuNPs

Qixin Liu [a,1], Ping Tang [b,1], Xinyue Xing [a], Wendai Cheng [a], Shengde Liu [a], Xiaoxu Lu [a,**], Liyun Zhong [b,*]

[a] Guangdong Provincial Key Laboratory of Nanophotonic Functional Materials and Devices, South China Normal University, Guangzhou, 510006, China
[b] Guangdong Provincial Key Laboratory of Photonics Information Technology, Guangdong University of Technology, Guangzhou, 510006, China

ARTICLE INFO

Keywords:
H_2O_2
Model enzyme
Colorimetry
SERS
Fe_3O_4@AuNPs

ABSTRACT

Hydrogen peroxide (H_2O_2) detection with high sensitivity plays an important role in biomedical research and food engineering. By combining colorimetry and surface enhanced Raman spectroscopy (SERS), we synthetize a novel H_2O_2 dual-sensor constructed via TMB–Fe_3O_4@AuNPs. In the presence of H_2O_2, the peroxide model enzyme might catalyze the oxidation of 3,3′,5,5′- tetramethylbenzidine (TMB) as blue charge transfer complex (CTC) for colorimetry, and then facilitate the sensitivity improvement of SERS detection. The achieved results show that in colorimetry, the linear range is from 40 μM to 5.5 mM with the detection limit of 11.1 μM; in SERS detection, the linear range is from 2 nM to 1 μM with the detection limit of 0.275 nM. Clearly, this mutual reference strategy improves both the detection limit of colorimetry and the sensitivity of SERS detection. Moreover, this colorimetry/SERS dual-sensor constructed via TMB–Fe_3O_4@AuNPs is successfully applied to the H_2O_2 detection in plasma and milk, indicating the excellent performance and flexibility.

1. Introduction

Hydrogen peroxide (H_2O_2), a common oxidant and essential intermediate or final product in food, is widely used in biomedicine, pharmacy, industry, environment and enzymatic reaction [1–4]. Actually, if the intake concentration of H_2O_2 is high or the intracellular H_2O_2 concentration exceeds 700 nM, human health is in danger [5,6], so it is required that the limit of detection (LOD) of H_2O_2 reaches nM level. To date, various H_2O_2 detection methods are proposed, including fluorescence [7], electrochemical method [8], high performance liquid chromatography [9] and colorimetry [10,11], etc. Among the above methods, H_2O_2 colorimetry, which reveals obvious advantages in low cost, simple operation, and good practicability, has been widely applied [12,13] while its LOD is only μM level [14–16]. Fluorescence-based H_2O_2 detection method has low LOD, but its result is usually affected by the autofluorescence background [17]. Compared with the fluorescence method, surface-enhanced Raman spectroscopy (SERS) shows obvious advantages in photobleaching resistance, self-quenching, single molecule LOD [18–20] and multiplexing detection [21,22], so it is becoming a fast and ultra-sensitive detection tool in food and biomedicine research [23–25].

3,3′,5,5′- tetramethylbenzidine (TMB), a most common colorimetric indicator of H_2O_2 [26,27], usually cause resonance Raman signal under the laser excitation of 632.8 nm [28]. When the reaction of TMB and H_2O_2 is implemented, both the color variation and Raman signal variation will appear, which will provide a mutual reference strategy for H_2O_2 detection. Since the intensity of Raman bands is proportional to the amount of charge transfer complex (CTC) [29,30], by combining the advantages of colorimetry in simplicity and practicability and SERS technique in low LOD, a high sensitivity H_2O_2 nanosensor with two mutual reference strategy will be constructed.

As shown in Fig. 1, we renew previous method to prepare Fe_3O_4@AuNPs [31]. By using bare Fe_3O_4 reserving the catalytic function of the simulated enzyme of nanoparticle, a “hot spot” of local electric field between AuNPs distributed on the surface of Fe_3O_4 particles is generated to realize Raman signal enhancement. And by controlling the growth size of AuNPs, we might adjust the local surface plasmon resonance (LSPR) peak to the excitation wavelength, thus Raman signal

* Corresponding author.
** Corresponding author.
E-mail addresses: hsgdzlxx@scnu.edu.cn (X. Lu), zhongly@gdut.edu.cn (L. Zhong).
[1] These authors contributed equally to this work.

https://doi.org/10.1016/j.talanta.2021.123118
Received 18 August 2021; Received in revised form 22 November 2021; Accepted 28 November 2021
Available online 16 December 2021

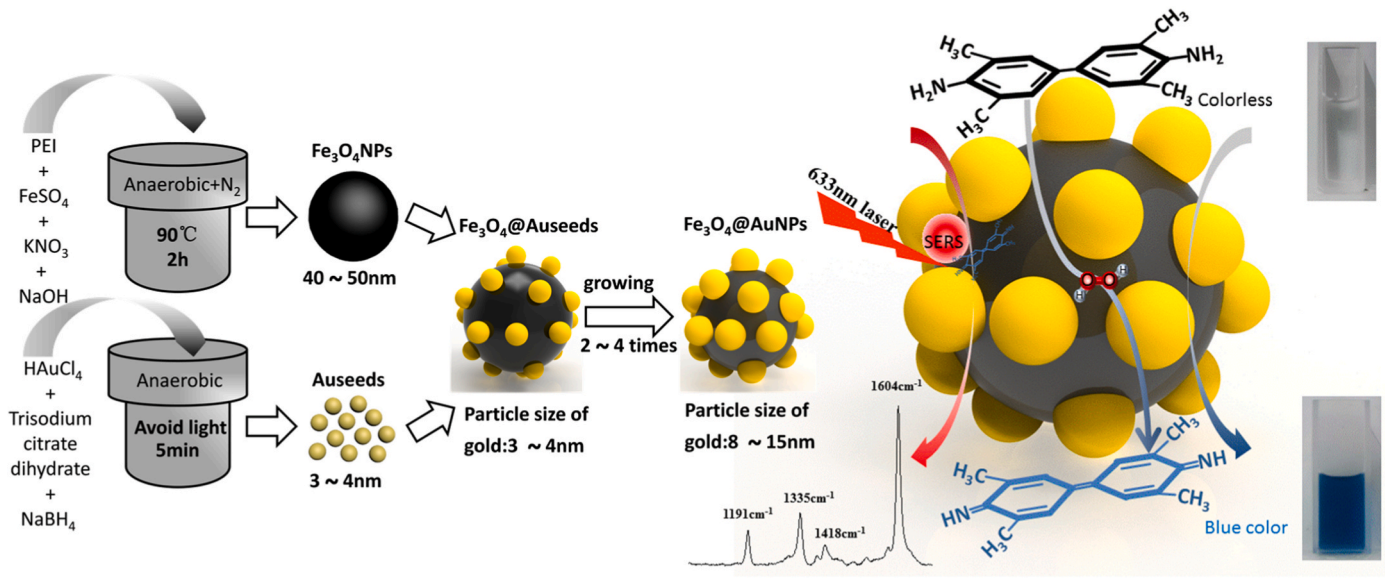

Fig. 1. Schematic illustration for the synthesis of Fe_3O_4@AuNPs and principle of colorimetric/SERS dual-sensor of H_2O_2 constructed via TMB-Fe_3O_4@ AuNPs.

enhancement can be further improved [29]. Moreover, under the action of magnetic field, Fe_3O_4@AuNPs will be aggregated reversibly, and the coupling effect of LSPR will appear among the aggregated particles, the "hot spots" enhancement is further improved [32]. Collectively, by introducing Fe_3O_4@AuNPs magnetic beads, we hope to construct a novel H_2O_2 nanosensor with two mutual reference strategy, in which not only the remarkable catalytic performance of Fe_3O_4 can be reserved, but also the distribution density of AuNPs on Fe_3O_4 nanoparticle surface will be increased and then SERS enhancement factor is improved. Following, we will present the corresponding theoretical analysis and experimental result.

2. Experimental section

2.1. Materials and reagents

Ferrous sulfate heptahydrate ($FeSO_4{\cdot}7H_2O$), sodium borohydride ($NaBH_4$), tetrachloroauric acid ($HAuCl_4$), polyethyleneimine (PEI), nitric acid (HNO_3), sodium citrate, cetyltrimethylammonium chloride (CTAC), potassium bromide (KBr) and L-ascorbic acid were purchased from Maclin (Shanghai, China); 3,3′,5,5′-tetramethylbenzidine (TMB) was achieved from Dalian Meilun Biotechnology Co., Ltd.; H_2O_2 (relative mass fraction 30%) and sodium hydroxide (NaOH) were purchased from Guangzhou Chemical Reagent Factory. All chemical reagents were analytically pure and might be directly used without further purification. The deionized water (with the resistivity of 18.2 MΩ·cm) was chosen.

2.2. Preparation of Fe_3O_4@AuNPs

Preparation of Fe_3O_4 nanoparticles. First, 65 mL deionized water was heated to 90 °C in oxygen-free environment filled with nitrogen. Second, 5 mL PEI solution (80 mg/mL), 10 mL $FeSO_4{\cdot}7H_2O$ aqueous solution (containing 1.280g$FeSO_4{\cdot}7H_2O$), 10 mL KNO_3 (2.0 M), 10 mL NaOH (1.0 M) were added and reacted for 2 h. The magnet settled and washed with deionized water for 5 times. 80 mL deionized water was added to resuspending.

Preparation of Auseeds . First, 1 mL 1% $HAuCl_4$ was added to 90 mL deionized water, and after stirring for 1min, 2 mL of sodium citrate solution (38.8 mM) and 1 mL solution containing $NaBH_4$ (0.075%) and sodium citrate (38.8 mM) were added. After stirring for 5min, the red Auseeds solution was achieved and stored it at 4°Cfor keeping away from light [31].

Preparation Fe_3O_4@AuNPs . First, 200 μL Fe_3O_4 solution was added to 9 mL Auseeds solution, and then the ultrasound treatment was intermittently implemented for 2 min at 8 min intervals for 2 h. Second, the deionized water was separated by magnet for 5 times, 9 mL was added to resuspending, then 1 mL Pei solution (80 mg/mL) was added, and the mixture was heated at 60 °C in the water bath for 1 h. Third, 5 mL of CTAC (0.1 M) solution was added to the resuspension, and ultrasonic treatment was carried out for 2min.

Growth of Fe_3O_4@AuNPs. Referring to the core-shell growth solution in previous reports [31]: Auseeds solution was added to Fe_3O_4@AuNPs solution, treated with ultrasonic wave for 3min and then reacted for 10min; 125 μL of HAuCl (10 mM) and 50 μL L-ascorbic acid (0.04 M) were added and treated with ultrasonic wave for 1min and then reacted for 10min. Repeated the above procedure for 2–5 times, the thickness of core-shell and the redshift of absorption peak of Fe_3O_4@AuNPs could be controlled.

2.3. Simulation of electromagnetic field around Fe_3O_4@AuNPs

Finite difference time domain (FDTD) method (Lumericfdtd, version 8.16) was used to perform the electromagnetic field calculation. On the basis of the statistical average size of TEM imaging, the diameter of Fe_3O_4 was set as 40 nm, the diameters of Auseeds were respectively set as 6 nm and 8 nm, and Auseeds were embedded in the surface of Fe_3O_4 for 0.5 nm. The incident direction of excitation laser (633 nm) was set as *Z*-axis and the polarization direction was located in *X*-axis; the incident electric field was 1 V/m, the dielectric constant of the material referred to previous work [33,34], and the refractive index of the background was set as 1.3334 of water.

2.4. H_2O_2 detection

First, different concentrations H_2O_2 solutions were achieved with acetic acid buffer (pH = 5). Second, 1 mL H_2O_2 with different concentrations (0–10 mM in colorimetry; and 0 -10μM in Raman method) were respectively placed into test tube, and then 0.5 mL Fe_3O_4@AuNPs and 1 mL TMB(10 mM) were added into the corresponding test tube. Third, each H_2O_2 solution was divided into two parts. One part was for the absorbance detection by the UV–Vis spectrophotometer and the other part was measured for Raman spectrum.

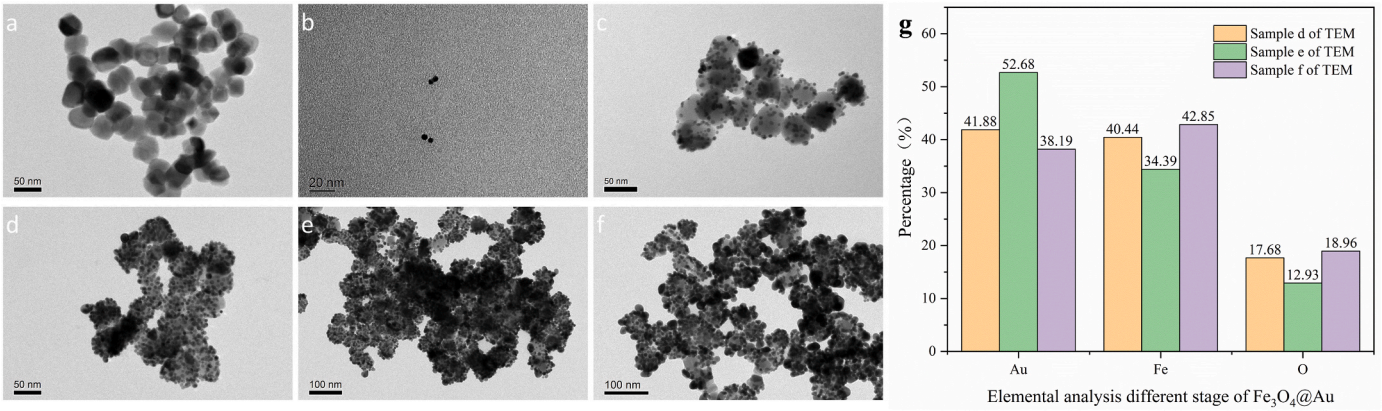

Fig. 2. The structure of the synthesized Fe_3O_4, Auseeds and Fe_3O_4@AuNPs:(a) Fe_3O_4; (b) Auseeds; (c) Fe_3O_4 @AuNPs; (d) Fe_3 O_4@AuNPs with firstgrowth of Auseeds; (e) Fe_3O_4@AuNPs with second growth of Auseeds; (f) Fe_3O_4@AuNPs nanoparticles with third growth of Auseeds; (g)EDS of sample e/d/f.growth of Auseeds; (g)EDS of sample e/d/f.

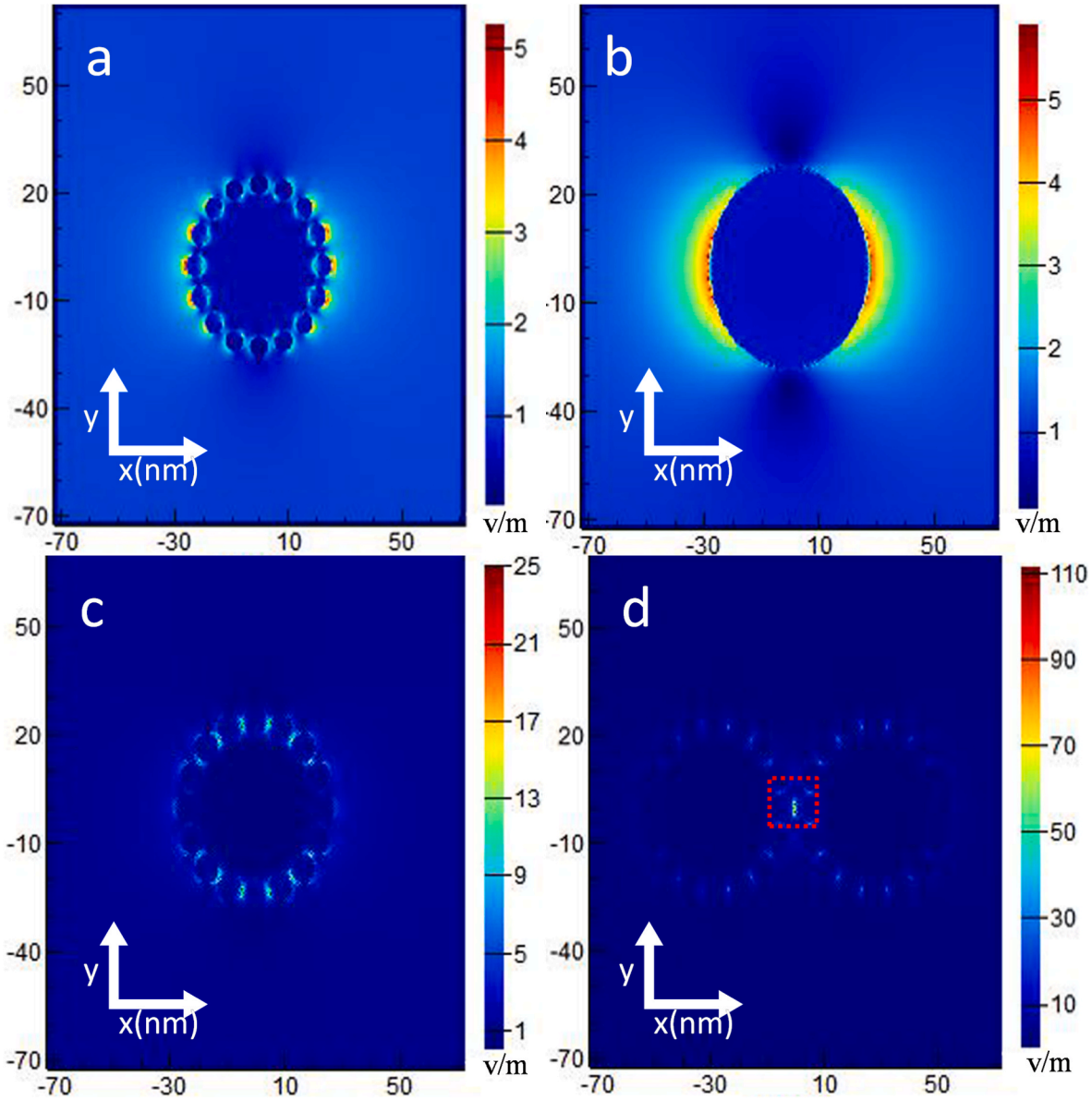

Fig. 3. FDTD numerical simulation results of electromagnetic field intensity distribution: (a) single Fe_3O_4@AuNPs (6 nm); (b) AuNPs(55 nm); (c) single Fe_3O_4@AuNPs(8 nm); (d) Fe_3O_4@AuNPs (8 nm) dimer.

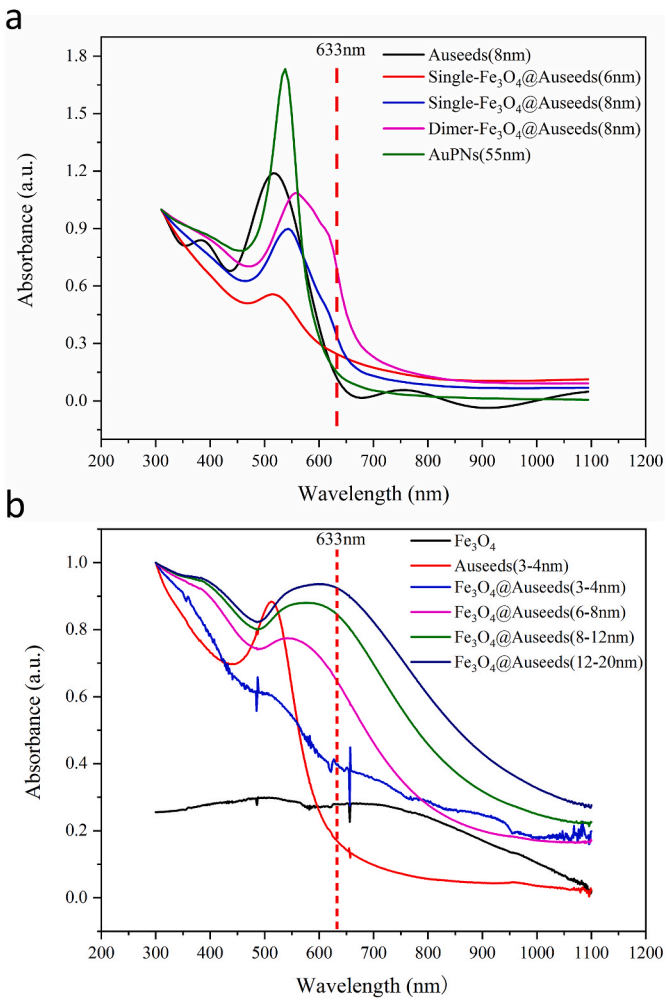

Fig. 4. (a)UV–vis spectrum of an 8 nm Auseed and above corresponding nanostructures; (b)The Auseeds and Fe_3O_4@AuNPs.

2.5. H_2O_2 detection in different samples

Referred to previous work [14] for milk pre-treatment steps. First, 5 mL of milk sample was added into a centrifuge tube (10 mL) and centrifuged at 10,000 rpm for 20min. Second, 2.5 mL supernatant and 2.5 mL deionized water were added to a 10 mL centrifuge tube, and centrifuged for 20min. Third, the supernatant was filtered through a 0.22 mm membrane. The pre-treatment of blood sample was similar to previous report [35]: Plasma was separated from blood at 10000 rpm for 20min.

3. Results and discussion

3.1. Characterization of Fe_3O_4@AuNPs

As shown in Fig. 2, the synthesized Fe_3O_4 nanoparticles were relatively uniform with the diameter of 40–50 nm. The initial particles of Auseeds were mostly in the size of 3–4 nm Fe_3O_4 nanoparticles were conjugated with Auseeds modified by PEI to form Fe_3O_4@Auseeds. In the beginning, the size of Auseeds on the surface of Fe_3O_4 nanoparticles was small and the distribution was relatively sparse. After the first growth, the size of Auseeds was about 6.3 nm, and the corresponding distribution became denser. After the second growth, the surface Auseeds were further dense, and the size of Auseeds was about 8.0 nm. After the third growth, the size of Auseeds became nonuniform while their sizes were increased with the maximum of 15 nm. As shown in Fig. 2(g), the energy dispersive spectrum (EDS) was used to explain the variation of Auseeds content during the iterative growth. It was found that the Auseeds content after 3-time additions Auseeds was 41.88%, 52.68% and 38.19%, respectively. Compared with the first Auseeds addition, the ratio of Au to Fe particles in the second Auseeds addition was significantly increased. However, in the third Auseeds addition, the ratio of Au to Fe was reduced relative to the second Auseeds addition, even less than the first Auseeds addition. Actually, along with the increasing of Auseeds, the adsorption capacity of PEI on Auseeds was limited. Meanwhile, these large Auseeds ran against each other and fell from the surface of Fe_3O_4. As shown in Fig. 2(f), a lot of bare areas on the surface of Fe_3O_4 were observed after the third Auseeds addition.

3.2. Simulation of electromagnetic field and UV–Vis spectrum of Fe_3O_4@AuNPs

In SERS, due to the proximity of molecules and surface plasmon matrix, free electrons on the surface of nano-metal structure collectively oscillated, thus the electromagnetic field enhancement appeared in local areas [36,37], and then Raman signal was improved [38]. To verify the electromagnetic enhancement effect of the synthesized Fe_3O_4@AuNPs, we first calculated the corresponding enhancement factor (EF), as shown in Fig. 3. Fig. 4 presented both the experimental and simulated UV–Vis spectra, it indicated the simulated result was basically consistent with

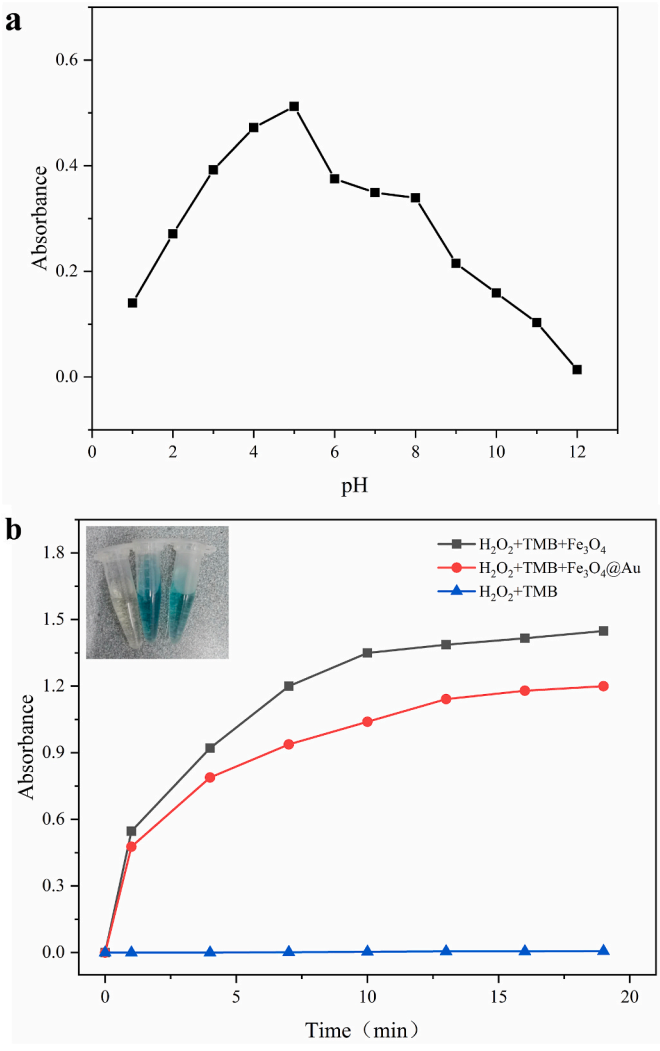

Fig. 5. (a)The relationship between enzyme activity and pH; (b)The relationship between time and reaction degree in different systems.

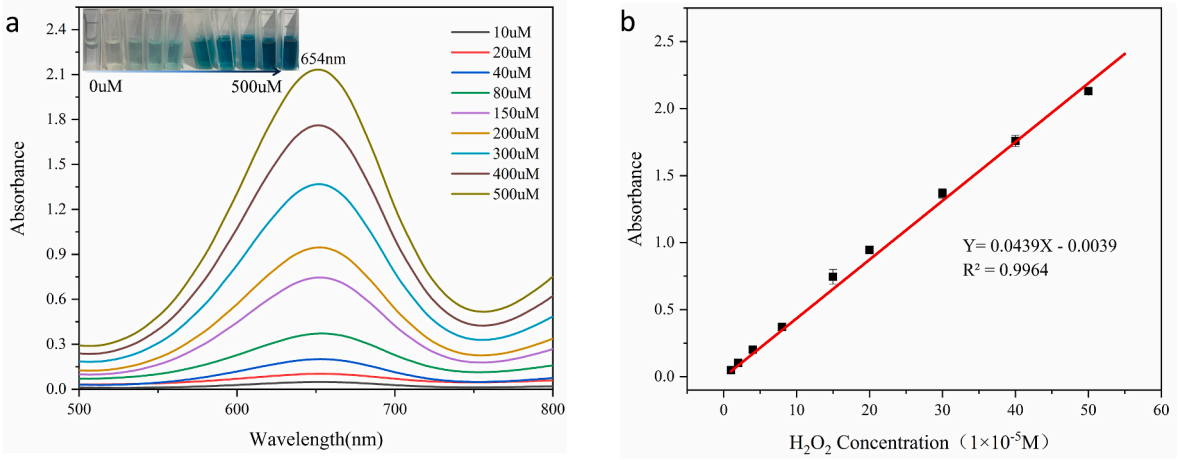

Fig. 6. (a) Corresponding U V -vis spectrum under different H_2O_2 concentrations; (b)The linear relationship between the absorption peak at 654 nm and the cone ent r ation o f H_2O_2.

the experimental result.

To compare the influence of the growth diameter of Auseeds on the surface of Fe_3O_4 particles on the SERS enhancement factor (SERS-EF), two diameters of Auseeds of 6 nm and 8 nm were set for simulation calculation. As shown in Fig. 3, when the diameter of Auseeds on the surface of Fe_3O_4 particles was varied from 8 nm to 6 nm, the intensity of local electric field between Auseeds became weak from maximum electric field intensity (Emax) 25 V/m to 5.2 V/m. In contrast, the result of Au nanoparticle with diameter of 55 nm was shown in Fig. 3(b), in which the Emax was about 5.7 V/m that was less than the result generated by same size Fe_3O_4@AuNPs. In Fig. 4(a), the peak position of simulated UV–Vis spectrum by single Fe_3O_4@Auseeds (8 nm) appeared obvious redshift due to the coulomb force between adjacent Auseeds particles, thus the plasma oscillations were coupled each other, and the oscillation mode of surface plasmon that was similar to the shell structure as a whole became stronger, so the redshift of surface plasmon resonance peak appeared.

As shown in Fig. 3(d), a “hot spot” was generated at the gap of a dimer, in which the intensity was about 114 times relative to original Emax and the EF (EF = $|E_{loc}/E_0|^4$, E_{loc} is the local electric field and E_0 is the incident electric field.) was about 1.69×10^8 [39]. Like previous report [40], this result further demonstrated that the action of external magnetic field can facilitate e nanoparticles aggregation, and then further improve SERS effect.

Actually, there was a positive correlation between SERS-EF and nanoparticle density [40]. To ensure the feasibility of the method, the Au density in FDTD simulation was set based on the average density in TEM image. Considering when the particle size of Auseeds was large, the catalytic effect of Fe_3O_4 on H_2O_2-TMB system was affected by various factors, such as the intensity of electromagnetic field and the UV–Vis spectrum in FDTD simulation, we selected Fe_3O_4-Aueeds nanoparticles grown twice for probe preparation.

3.3. *Enzyme activity of Fe_3O_4@AuNPs*

As mentioned above, the structure of Fe_3O_4@AuNPs might affect the catalytic activity of Fe_3O_4. Therefore, we compared the absorbance variation of Fe_3O_4, H_2O_2-TMB-Fe_3O_4 and H_2O_2-TMB-Fe_3O_4@AuNPs during 20 min reaction. As shown in Fig. 5(a), it was found that the H_2O_2-TMB (10^{-4}nM) solution without catalyst was colorless, and no obvious difference between H_2O_2-TMB(10^{-4}nM) with Fe_3O_4 and H_2O_2-TMB (10^{-4}nM) with Fe_3O_4@AuNPs was observed. In order to get the optimum reaction conditions, the effect of pH on the enzyme activity of Fe_3O_4 was examined in the range of pH 1–12 (Fig. 5(b)). We can see that the catalytic activity of Fe_3O_4 was improved with the increasing pH value until 5, then decreased with the increasing of pH value, and the reaction time with maximum catalytic activity was about 18 min.

3.4. *Colorimetry and SERS detection of H_2O_2*

Colorimetry: Based on the catalytic characteristics of Fe_3O_4, we used Fe_3O_4@AuNPs as the catalyst of H_2O_2-TMB system to construct

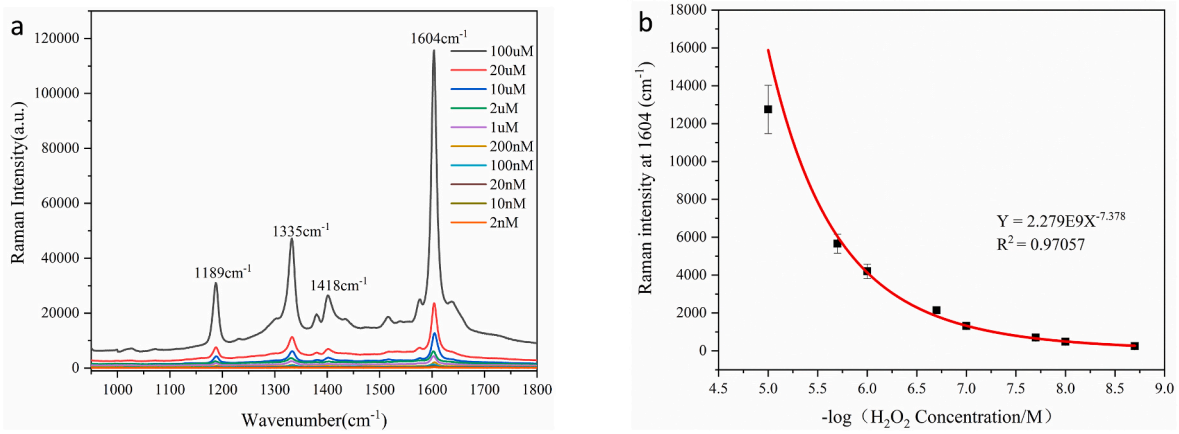

Fig. 7. (a)Raman spectra corresponding to different H_2O_2 concentrations; (b) The linear relationship between the Raman peak at 1604 cm^1 and the concentration of H_2O_2.

Table 1
Comparative study of H_2O_2 detection.

detection element	method	linear range	LOD	ref
Fe_3O_4@SiO_2–NH_2-Au@Pd0.30NPs	colorimetric	0.010–60	0.060 μM	[41]
Fe_3O_4@SiO_2@Au nanocomposite	colorimetric	5-35 μM	3 μM	[42]
Fe/CuSn$(OH)_6$	colorimetric	30-1000 μM	9.49 uM	[14]
Fe Pt–Au HNPs	colorimetric	20-700 μM	12.33 uM	[15]
Mn_2CuO_4	electrochemical	0.036–9300 μM	0.013 μM	[16]
Ag–Cu_2O/Reduced Graphene Oxide Nanocomposites	SERS	10^{-2}-10^{-8}M	1.6*10^{-8}M	[30]
Fe_3O_4@AuNPs	colorimetric	4-550 μM	11.1 μM	This work
	SERS	2–10000 nM	0.275 nM	This work

colorimetry/SERS dual-sensors. Color variation of the catalytic system was shown in the inset of Fig. 6. We can see that along with the increasing of H_2O_2 concentration, the solution color was gradually changed from colorless to blue, and the absorbance of TMB containing H_2O_2 was measured by UV–Vis spectrophotometer. As shown in Fig. 6 (b), along with the increasing of H_2O_2 from 40uM-5.5 mM, the intensity of absorption peak at 654 nm was significantly increased. Fig. 6(b) presents the absorbance variation with H_2O_2 concentration, the detection limit reached 11.1 μM in the range of 40uM-5.5 mM($R^2 = 0.996$).

SERS detection: As shown in Fig. 7(a), a typical band at 1418 cm^{-1} was observed in the Raman spectrum of oxidized TMB which was classified as unoxidized diamine [34]. And in the presence of H_2O_2, the bands at 1189, 1335 and 1604 cm^{-1} also appeared, assigned to CH_3 bending modes, inter-ring C–C stretching modes, ring stretching and C–H bending modes, respectively [28]. Thus, CTC can be characterized by three fingerprints peaks of 1189,1135,1604 cm^{-1} [28]. Moreover, the typical band of TMB was still observed at 1418 cm^{-1} under high H_2O_2 concentration and TMB, indicating that a few TMB molecules were not oxidized.

Like colorimetry, Raman signal variation also can be used to monitor H_2O_2 concentration. Along with the increasing of H_2O_2 concentration, Raman signal intensity of CTC become strong under 633 nm laser excitation (Fig. 7(a)). From Raman spectrum of CTC generated by the catalytic reaction of TMB under different concentrations H_2O_2 (2 nM -1uM), it was found that along with the increasing of H_2O_2concentration, Raman peak at 1604 cm^{-1} was gradually increased. Fig. 7(b) showed the relationship between the intensity of Raman peak at 1604 cm^{-1} and H_2O_2 concentration. A good linear relationship can be found in the range of 2 nM-1uM ($R^2 = 0.971$), and the corresponding detection limit reached 0.275 nM.

Compared with current H_2O_2 detection methods, the proposed Fe_3O_4@AuNPs dual-sensor showed extremely low detection limit (0.275 nM) and large linear range (40μM-5.5 mM and 2 nM-1uM) (Table 1). In addition, since the magnetic property of nanoparticles can be used for effective separation and recovery, so we can simplify not only the procedure of centrifugal separation in colorimetry, but also realize reuse efficiently. Clearly, the excellent sensing performance in such colorimetry/SERS method was attributed to the high catalytic activity of Fe_3O_4@AuNPs and the enhancement of Raman signal by a stable electromagnetic field generated between Auseeds. In addition, this colorimetry/SERS could greatly reduce the error induced by the environmental variation and ensure the reliability of the measurement results by two mutual reference strategy.

3.5. Recoverability examination

As stated above, Fe_3O_4@AuNPs showed good catalytic stability and recoverability, and they might be aggregated and separated from the system by external magnetic force. The recoverability was examined in the presence of 1 mL of H_2O_2 (1×10^{-3} M). Fig. 8(a) presented the Raman spectrum of the reaction between H_2O_2 and TMB catalyzed by the recovered Fe_3O_4@AuNPs. The intensity of the SERS signal was decreased with the used number. Fig. 8(b) showed the recovery process of Fe_3O_4@AuNPs, and the UV–Vis spectrum between H_2O_2 and TMB reaction revealed good catalytic activity of probe, which reflected that Fe_3O_4@AuNPs was indeed a good reusable catalyst and SERS substrate.

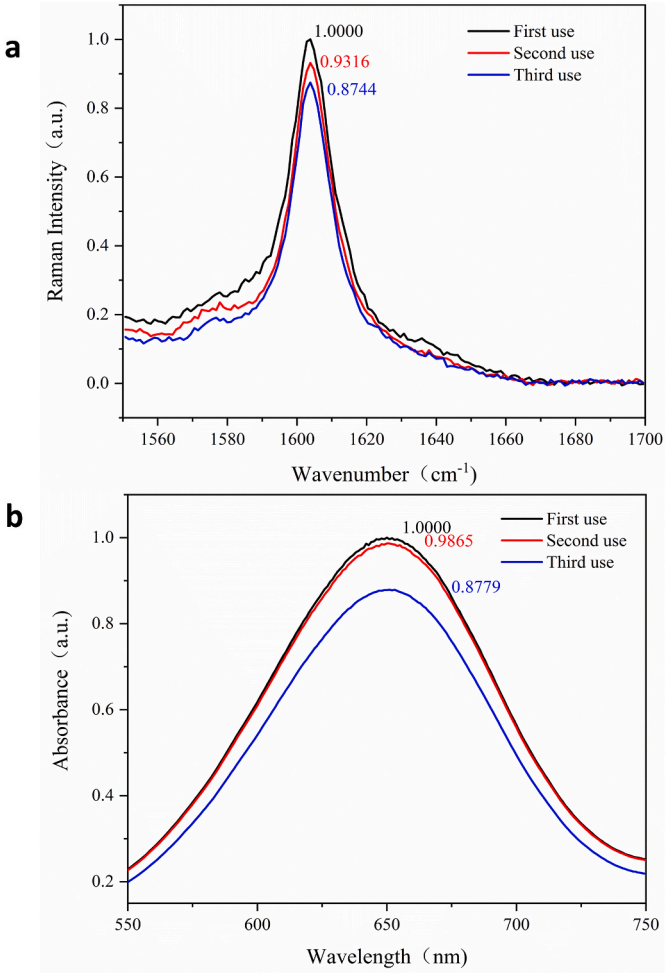

Fig. 8. The relationship between usage times and spectral intensity: (a)Raman spectrum; (b)UV–vis spectrum.

3.6. Real sample examination

To verify the flexibility of TMB-Fe_3O_4@ AuNPs, we examined H_2O_2 concentrations in plasma and milk samples. As shown in Table 1. All samples were analyzed by colorimetry. The recovery was in the range of 104.14 and 113.89%, and the relative standard deviation was varied from 2.87 to 9.18%. In contrast, the SERS method was utilized to examine H_2O_2 concentrations in plasma and milk samples, respectively. When the H_2O_2 (1×10^{-6} M and 2×10^{-7} M) were respectively added to the plasma and milk samples, the corresponding recoverability was 93.42 and 140.01%, and the relative standard deviations were varied from 2.16 to 23.58% (Table 2). These results demonstrated good performance of the dual colorimetry/SERS sensor constructed by TMB-Fe_3O_4@AuNPs in H_2O_2detection. Furthermore, such colorimetric/SERS sensor was also used to verify the difference between health and unhealth samples. As shown in Fig. 9, we set 700 nM as the reference line corresponding to Raman intensity of 3426.7 (a.u.) and the Raman intensity more than and less than 700 nM were respectively defined as

Table 2
Consequents of real sample analysis.

method	sample	added H_2O_2 (uM)	detected H_2O_2(uM)			recovery (%)			relative standard deviation (RSD) (%)		
colorimetric	Milk 1、2、3	200.00	211.59	226.85	227.77	105.79	113.42	113.89	3.98	8.90	9.18
	Plasma 1、2、3	250.00	260.34	276.97	277.42	104.14	110.79	110.97	2.87	7.24	7.35
SERS	Milk a、b、c	0.20	0.21	0.27	0.28	103.11	134.95	140.01	2.16	21.04	23.58
	Plasma a、b、c	1.00	0.93	1.34	1.15	93.42	133.55	115.14	4.81	20.32	9.95

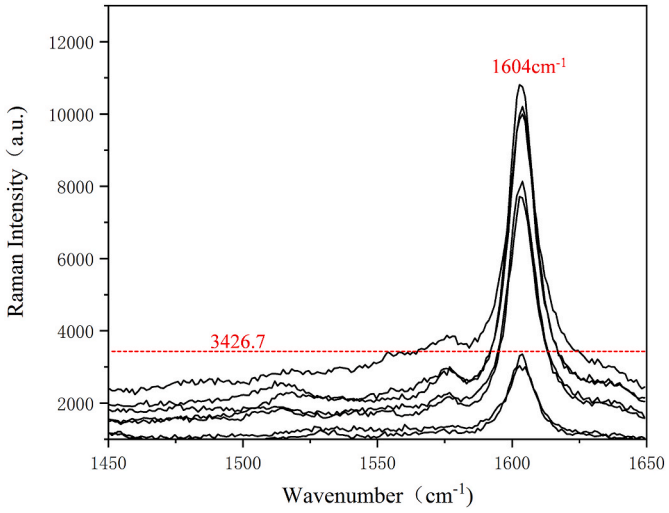

Fig. 9. Experiments to differentiate between health and unhealth samples.

the unhealthy and healthy samples. Clearly, the experimental result was coincident with the state of the preset sample very well.

4. Conclusion

In this work, using TMB and Fe_3O_4@AuNPs synthesized by a green and convenient water bath heating method, we construct a colorimetry/SERS dual-sensor of H_2O_2. The achieved result demonstrates that the high-density Au nano-assembly structure is very beneficial to improve Raman signal enhancement, in which the measuring range reaches 2 nM-1uM for SERS and 40uM-5.5 mM for colorimetry with the LOD of 0.275 nM, indicating obvious advantages of such colorimetry/SERS dual-sensor in sensitivity, catalytic activity, flexibility and recoverability. Importantly, this colorimetry/SERS dual-sensor will provide a mutual reference strategy in glucose and lactic acid detection, environmental monitoring and food engineering.

Credit author statement

I declare that this thesis and its research work were completed by the author of this article. The research materials used in the completion of this thesis are listed in the references; strictly abide by the relevant national confidentiality regulations, there is no phenomenon of multiple submissions. After publishing, I would bear my own responsibility.

Declaration of competing interest

The authors declare that they have no known competing financial interests or personal relationships that could have appeared to influence the work reported in this paper.

Acknowledgments

This work is supported by the National Nature Science Foundation of China (grants: 61875059 and 61727814).

References

[1] N.H. Martin, A. Friedlander, A. Mok, D. Kent, K. Wiedmann, M. Boor, Peroxide test strips detect added hydrogen peroxide in raw milk at levels affecting bacterial load, J. Food Protect. 77 (2014) 1809–1813.
[2] M.P. Murphy, A. Holmgren, N.G. Larsson, B. Halliwell, C.J. Chang, B. Kalyanaraman, S.G. Rhee, P.J. Thornalley, L. Partridge, D. Gems, T. Nystrom, V. Belousov, P.T. Schumacker, C.C. Winterbourn, Cell Metabol. 13 (2011) 361–366.
[3] S. Muralikrishna, S. Cheunkar, B. Lertanantawong, T. Ramakrishnappa, D. H. Nagaraju, W. Surareungchai, R.G. Balakrishna, K.R. Reddy, Graphene oxide-Cu (II) composite electrode for non-enzymatic determination of hydrogen peroxide, J. Electroanal. Chem. 776 (2016) 59–65.
[4] Yang Xuejing, Duan Yanghua, Wang Jinling, Wang Hualin, Liu Honglai, David L. Sedlak, Impact of peroxymonocarbonate on the transformation of organic contaminants during hydrogen peroxide in situ chemical oxidation, J. Environmental Science & Technology Letters 6 (12) (2019) 781–786.
[5] J.M. Desesso, A.L. Lavin, S.M. Hsia, R.D. Mavis, Assessment of the carcinogenicity associated with oral exposures to hydrogen peroxide, Food Chem. Toxicol. 38 (2000) 1021–1041.
[6] M. Valko, D. Leibfritz, J. Moncol, M.T.D. Cronin, M. Mazur, J. Telser, Free radicals and antioxidants innormal physiological functions and human disease, Int. J. Biochem. Cell Biol. 39 (2007) 44–84.
[7] B.C. Dickinson, C.J. Chang, A targetable fluorescent probe for imaging hydrogen peroxide in the mitochondria of living cells, J. Am. Chem. Soc. 130 (2008) 9638–9639.
[8] F. Xu, M. Deng, G. Li, S. Chen, L. Wang, Electrochemical behavior of cuprous oxide-reduced graphene oxide nanocomposites and their application in nonenzymatic hydrogen peroxide sensing, Electrochim. Acta 88 (2013) 59–65.
[9] M. Tarvin, B. McCord, K. Mount, K. Sherlach, M.L. Miller, Optimization of two methods for the analysis of hydrogen peroxide: high performance liquid chromatography with fluorescence detection and high-performance liquid chromatography with electrochemical detection in direct current mode, J. Chromatogr. A 1217 (2010) 7564–7572.
[10] H. Liu, Y. Ding, B. Yang, Z. Liu, Q. Liu, X. Zhang, Colorimetric and ultrasensitive detection of H_2O_2 based on Au/Co_3O_4-CeO_x nanocomposites with enhanced peroxidase-like performance, Sens. Actuators, B 271 (2018) 336–345.
[11] H. Wei, E. Wang, Fe_3O_4 magnetic nanoparticles as peroxidase mimetics and their applications in H_2O_2 and glucose detection, Anal. Chem. 80 (2008) 2250–2254.
[12] Q. Liu, P. Chen, Z. Xu, M. Chen, Y. Ding, K. Yue, J. Xu, A facile strategy to prepare porphyrin functionalized ZnS nanoparticles and their peroxidase-like catalytic activity for colorimetric sensor of hydrogen peroxide and glucose, Sens. Actuators, B 251 (2017) 339–348.
[13] Y. Yin, C. Gao, Q. Xiao, G. Lin, Z. Lin, Z. Cai, H. Yang, Protein-metal organic framework hybrid composites with intrinsic peroxidase-like activity as a colorimetric biosensing platform, ACS Appl. Mater. Interfaces 8 (2016) 29052–29061.
[14] H. Liu, Y.N. Ding, B. Yang, Z. Liu, X. Zhang, Q.Y. Liu, Iron doped $CuSn(OH)_6$ microspheres as a peroxidase-mimicking artificial enzyme for H_2O_2 colorimetric detection, ACS Sustain. Chem. Eng. 6 (2018) 14383–14393.
[15] Y. Ding, B. Yang, H. Liu, Z. Liu, X. Zhang, X. Zheng, Q. Liu, FePt-Au ternary metallic nanoparticles with the enhanced peroxidase-like activity for ultrafast colorimetric detection of H_2O_2, Sens. Actuators, B 259 (2018) 775–783.
[16] P. Balasubramanian, M. Annalakshmi, S. Chen, T. Sathesh, T. Peng, T.S. T. Balamurugan, Facile solvothermal preparation of Mn_2CuO_4 microspheres: excellent electrocatalyst for real-time detection of H_2O_2 released from live cells, ACS Appl. Mater. Interfaces 10 (2018) 43543–43551.
[17] J.J. Gao, H. Liu, L.Y. Pang, K. Guo, J.Q.Y. Li, Biocatalyst and colorimetric/fluorescent dual biosensors of H_2O_2 constructed via hemoglobin–$Cu_3(PO_4)_2$ organic/inorganic hybrid nanoflowers, ACS Appl. Mater. Interfaces 10 (2018) 30441–30450.
[18] M.J. Baker, K. Faulds, Fundamental developments in clinical infrared and Raman spectroscopy, Chem. Soc. Rev. 45 (2016) 1792–1793.
[19] L.A. Lane, X. Qian, S. Nie, SERS nanoparticles in medicine: from label-free detection to spectroscopic tagging, Chem. Rev. 115 (2015) 10489–10529.
[20] S. Nie, S.R. Emery, Probing single molecules and single nanoparticles by surface-enhanced Raman scattering, Science 275 (1997) 1102–1106.
[21] Y.C. Cao, R.C. Jin, C.A. Mirkin, Nanoparticles with Raman spectroscopic fingerprints for DNA and RNA detection, Science 297 (2002) 1536–1540.
[22] W. Zhou, Q. Li, H. Liu, J. Yang, D. Liu, Building electromagnetic hot spots in living cells via target-triggered nanoparticle dimerization, ACS Nano 11 (2017) 3532–3541.

[23] K. Sivashanmugan, K. Squire, A. Tan, Y. Zhao, J.A. Kraai, G.L. Rorrer, A.X. Wang, Trace detection of tetrahydrocannabinol in body fluid via surface-enhanced Raman scattering and principal component analysis, ACS Sens. 4 (2019) 1109.
[24] D. Li, X. Cao, Q. Zhang, X. Ren, L. Jiang, D. Li, W. Deng, H. Liu, Facile in situ synthesis of core–shell MOF@Ag nanoparticle composites on screen-printed electrodes for ultrasensitive SERS detection of polycyclic aromatic hydrocarbons, J. Mater. Chem. 7 (2019) 14108–14117.
[25] B. Zhao, S. Feng, Y. Hu, S. Wang, X. Lu, Rapid determination of atrazine in apple juice using molecularly imprinted polymers coupled with gold nanoparticles-colorimetric/SERS dual chemosensor, Food Chem. 276 (2019) 366–375.
[26] W. Qin, L. Su, C. Yang, Y. Ma, H. Zhang, X. Chen, Colorimetric detection of sulfite in foods by a TMB-O_2-Co_3O_4 nanoparticles detection system, J. Agric. Food Chem. 62 (2014) 5827–5834.
[27] G. Fu, S.T. Sanjay, W. Zhou, R.A. Brekken, R.A. Kirken, X. Li, Exploration of nanoparticle-mediated photothermal effect of TMB-H_2O_2 colorimetric system and its application in a visual quantitative photothermal immunoassay, Anal. Chem. 90 (9) (2018) 5930–5937.
[28] S. Laing, A. Hernandez-Santana, J.r. Sassmannshausen, D.L. Asquith, I.B. McInnes, K. Faulds, D. Graham, Quantitative detection of human tumor necrosis factor α by a resonance Raman enzyme-linked immunosorbent assay, Anal. Chem. 83 (2010) 297–302.
[29] J. Langer, D. Jimenez de Aberasturi, J. Aizpurua, R.A. Alvarez-Puebla, B. Auguié, J. J. Baumberg, G.C. Bazan, S.E.J. Bell, A. Boisen, A.G. Brolo, et al., Present and future of surface-enhanced Raman scattering, ACS Nano 14 (2020) 28–117.
[30] Y. Guo, H. Wang, X. Ma, J. Jin, W. Ji, X. Wang, W. Song, B. Zhao, C. He, Fabrication of Ag-Cu_2O/reduced graphene oxide nanocomposites as surface-enhanced Raman scattering substrates for in situ monitoring of peroxidase-like catalytic reaction and biosensing, ACS Appl. Mater. Interfaces 9 (2017) 19074–19081.
[31] I.Y. Goon, L.M.H. Lai, M. Lim, P. Munroe, J.J. Gooding, R. Amal, Fabrication and dispersion of gold-shell-protected magnetite nanoparticles: systematic control using polyethyleneimine, Chem. Mater. 21 (2009) 673–681.
[32] D. Yoo, K.L. Gurunatha, H.-K. Choi, D.A. Mohr, C.T. Ertsgaard, R. Gordon, S.-H. Oh, Low-power optical trapping of nanoparticles and proteins with resonant coaxial nanoaperture using 10 nm gap, Nano Lett. 18 (6) (2018) 3637–3642.
[33] H. Boppart, A.S.&P. Wachter, Optical Properties of Magnetite Fe_3O_4, J. Philosophical Magazine Part B, 1980.
[34] P.B. Johnson, R.W. Christy, Optical constants of the noble metals, J. Phys Rev B, Solid State (USA) 6 (12) (1972) 4370–4379.
[35] W. Premasiri, J. Lee, L. Ziegler, Surface-enhanced Raman scattering of whole human blood, blood plasma, and red blood cells: cellular processes and bioanalytical sensing, J. Phys. Chem. B 116 (2012) 9376–9386.
[36] E.C. Le Ru, P.G. Etchegoin, Principles of Surface-Enhanced Raman Spectroscopy and Related Plasmonic Effects, Elsevier, Amsterdam/Oxford, 2009.
[37] M. Moskovits, Surface-enhanced Raman spectroscopy: a brief retrospective, J. Raman Spectrosc. 36 (2005) 485–496.
[38] H. Raether, Surface Plasmons on Smooth and Rough Surfaces and on Gratings, Springer-Verlag, Berlin, 1988.
[39] L.K. Ausman, G.C. Schatz, On the importance of incorporating dipole reradiation in the modeling of surface enhanced Raman scattering from spheres, J. Chem. Phys. 131 (2009), 0847083.
[40] Stefen Stangherlin, Nicole Cathcart, Frederick Sato, Vladimir Kitaev, Gold nanoprisms: synthetic approaches for mastering plasmonic properties and implications for biomedical applications, ACS Appl. Nano Mater. 3 (8) (2020) 8304–8318.
[41] A. Omotayo, S. Sicwetsha, P. Mashazi, Nanomagnet-silica nanoparticles decorated with Au@Pd for enhanced peroxidase-like activity and colorimetric glucose sensing, J. ACS Applied Materials & Interfaces 12 (2) (2019) 1973–1987.
[42] S. Luo, Y. Liu, H. Rao, Y. Wang, X. Wang, Fluorescence and magnetic nanocomposite Fe_3O_4@SiO_2@Au MNPs as peroxidase mimetics for glucose detection, Anal. Biochem. 538 (2017) 26–33.